Journal of *Marine Science and Engineering*

MDPI

Article

Experimental Study of the Wave Effects on a Ducted Twin Vertical Axis Tidal Turbine Wake Development

Robin Linant [1,2], Yanis Saouli [1,2], Grégory Germain [1,*] and Guillaume Maurice [2]

[1] Ifremer, RDT Research and Technological Development, 62200 Boulogne-sur-Mer, France; robin.linant@ifremer.fr (R.L.); yanis.saouli@ifremer.fr (Y.S.)
[2] HydroQuest SAS, 16 Chemin de Malacher, 38240 Meylan, France; guillaume.maurice@hydroquest.net
* Correspondence: gregory.germain@ifremer.fr

Abstract: Horizontal-axis turbines have been well-studied; however, there is a serious lack of information on the behaviour of vertical-axis turbines under unsteady operating conditions. Among unsteady flows, waves can cause significant mechanical fatigue and modify the flow downstream of the tidal turbines. Consequently, this paper aims to characterize the effects of waves on the hydrodynamic performance and wake development of a 1/20 scale model of a ducted twin vertical axis 1 MW-rated demonstrator. Power measurements were taken from the turbine and the velocity measurements downstream of the machine using a three-component Laser Doppler Velocimeter. The results show that, in the presence of waves, the mean wake characteristics present greater average height and width compared to the current-only condition. Moreover, the wake recovery happens faster downstream due to the sheared wake region homogenization, induced by the presence of higher intensity vortices. Through the Turbulence Kinetic Energy estimation, we also observe some increased fluctuations around the turbine and close to the free surface due to the presence of waves.

Keywords: tidal energy; vertical axis turbine; tank tests; surface waves; wake; turbulence

Academic Editors: Decheng Wan and Abdellatif Ouahsine

Received: 20 December 2024
Revised: 13 February 2025
Accepted: 14 February 2025
Published: 18 February 2025

Citation: Linant, R.; Saouli, Y.; Germain, G.; Maurice, G. Experimental Study of the Wave Effects on a Ducted Twin Vertical Axis Tidal Turbine Wake Development. *J. Mar. Sci. Eng.* **2025**, *13*, 375. https://doi.org/10.3390/jmse13020375

1. Introduction

For several years, human activity has significantly increased its greenhouse gas emissions. To limit this growing phenomenon, electricity production based on renewable sources of energy is emerging, especially through the deployment of offshore wind and tidal turbines. Taking into account its predictability and its energy potential, a wide range of tidal turbine concepts are under development, confirming the high potential of tidal energy [1]. Through numerical and in situ studies [2], many sea sites seem to offer favourable environmental conditions for the installation of tidal farms. However, those sites are characterized by complex flow properties including high current velocity, changes in the flow direction, and highly sheared velocity profiles [3,4]. In addition, surface waves can severely affect the flow properties and accentuate the velocity fluctuations [5,6], leading to significant mechanical fatigue and reductions in performance, as well as changes in wake development.

Experimental and numerical approaches have been undertaken to study the wake development of turbine models [7,8] to ensure a good way of installing tidal farms. Ref. [9] displayed the influence of the turbulent intensity on Horizontal Axis Tidal Turbine (HATT) behaviour. Experimentally, they have shown that the evolution of the velocity deficit is conditioned by the turbulent intensity generated in the tank. In particular, the greater the turbulent intensity, the faster the wake recovery. A similar trend is exposed in [10] which

expect higher turbulence intensity to promote faster wake recovery. Ref. [11] characterize experimentally the steady flow direction effect on the wake of a twin Vertical Axis Tidal Turbine (2-VATT). This study highlights that the flow direction is responsible for a merging difference in the maximum velocity deficit. While most vertical-axis turbines operate with a single rotor, which limits their capacity to harness energy efficiently, especially with the H geometry rotor which is known to be less efficient in a single rotor configuration, the proposed system integrates four rotors on a single gravity-based structure, enhancing overall efficiency due to the fairing geometry. This multi-rotor configuration provides two main advantages: the counter rotation of the rotor columns effectively cancels out the tilting moment, ensuring greater structural stability; this counter rotation promotes enhanced internal wake mixing, which can help accelerate energy recovery of the downstream flow. This can lead to reduced turbine spacing, potentially increasing the overall production of tidal farms [12]. This aspect is particularly relevant compared to large-scale horizontal-axis farms, where wake recovery and spacing optimization remain key challenges. In general, further comparison to horizontal-axis tidal turbines in terms of production, vertical-axis turbines demonstrates better performance in shallow waters and turbulent flow conditions [13], where their energy capture ability, independent of the flow direction, mitigates misalignment losses.

The majority of studies on wave effects mainly concern the horizontal axis tidal turbines (HATT) [14–16]. It has been shown that the power output and mean thrust coefficient are not affected by the surface waves, but the standard deviation of the power and torque coefficients are harshly affected by the waves. Ref. [17] shows that the fluctuations of the power coefficient are cyclic and tend to oscillate at the wave frequency. Ref. [18] shows that the interaction between the oscillatory flow induced by the waves and the turbine could lead to better wake mixing in the near wake. Ref. [19] noticed that the turbulent intensity (TI) increases in the presence of waves, unlike the mean velocity deficit. Also, Ref. [20] shows that the waves increase the vertical flow mixing and enhance the stall of tip vortices, which are non-uniformly advected due to the wave-induced variation in velocity in the region of the flow between the turbine top-tip and the free surface. To the best of the authors' knowledge, the aforementioned experiments are mainly carried out on HATT and no study considered the wave effect on the wake development of 2-VATT.

To fill this gap, this study experimentally investigates the wake characteristics of a 2-VATT model subjected to wave and current interaction. A comparison study is conducted with a current-only case presented in [11] to better understand and predict the effects of waves on ducted vertical axis tidal turbines. Section 2 describes the experimental set-up used for the test campaign and the effect of waves on the overall hydrodynamic behaviour of the turbine. Section 3 presents the wave effects on the mean wake development and dynamics of the 2-VATT. And finally, the main results are discussed in the conclusion.

2. Material and Method

2.1. Turbine Model

The studied turbine is a 1/20 scale model of the 1 MW-rated demonstrator developed by HydroQuest and deployed at the Paimpol-Bréhat test site [21]. Two independent counter-rotating vertical axis rotor columns (Figure 1), composed of two levels of Darrieus-type rotors with a 60° phase difference between them, allow to capture the flow kinetic energy. Each rotor consists of N = 3 blades with NACA 0018 profiles, such that the blade height (H_{blade}) is 190 mm and the chord (c) is 73 mm. The rotor radius is $R = D/2$ = 200 mm, so the rotor's solidity S (Nc/R) is 1.1, like the full-scale demonstrator. The model has a width of W = 1.24 m between the two rotor columns. Its overall height, including the gravity

base, is H_{model} = 840 mm. For the remainder of the study, the distances are normalised by H = 450 mm for the height between the top and bottom horizontal plates.

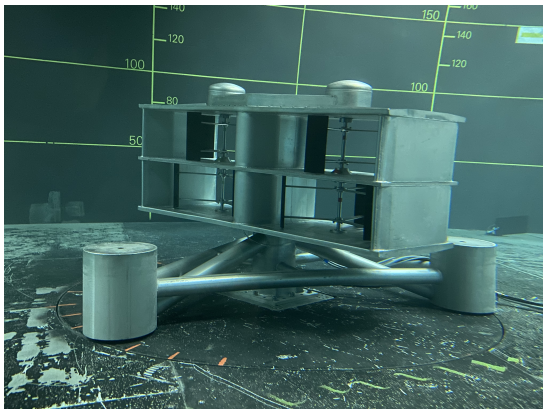

Figure 1. The 1:20 model of the HydroQuest's ducted 2-VATT immersed in the Ifremer's flume tank.

The electronics and transmission system are integrated into the turbine's waterproof central fairing. The rotors are driven by belts linking the drive shafts. The model is equipped with a Maxon RE50 DC motor, a 1/26 reducer, and a speed encoder (Figure 2). Remote Escon 70/10 servo-controllers are used to allow motor regulation in constant speed mode. The torque is measured with a Scaime DR2112-W torquemeter. The demonstrator's gravity base is represented by a pseudo-tripod base on which the turbine is fixed through a load cell (six-components SIXAXES 1.5 kN).

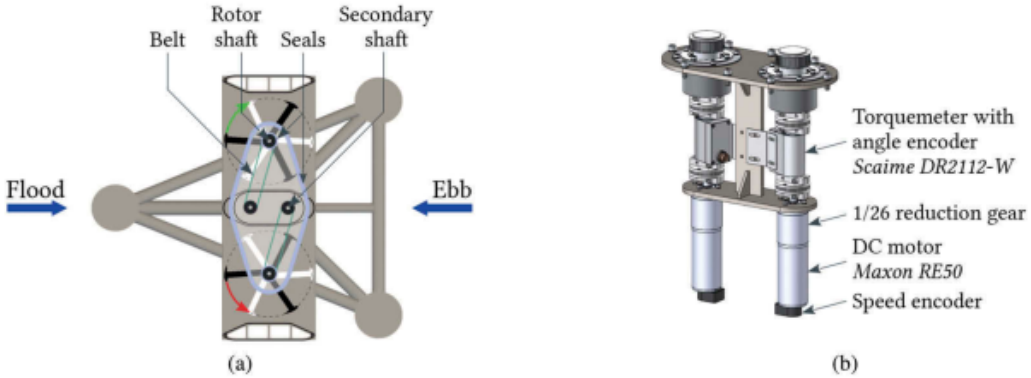

Figure 2. (**a**) CAD view of the twin counter-rotative VATT model with the transmission system on the top. (**b**) View of the regulation system located in the turbine's central fairing.

2.2. Experimental Setup

In order to study the impact of the waves on the ducted 2-VATT behaviour, tests were carried out on the wave and current circulating tank of IFREMER, in Boulogne-sur-Mer (France). The flume tank has a working Section 2 m deep (h_{wat}), 4 m wide (w_{wat}), and 18 m long. Two pumps ensured the motion of 700 m^3 of water to reach a current speed up to 2 m/s. Three instantaneous velocity components (U, V, W) are associated to the three directions $(\vec{x}, \vec{y}, \vec{z})$. Initially, the incoming flow $(U_\infty, V_\infty, W_\infty)$ is supposed to be constant and steady. A *Dantec* 3-component Laser Doppler Velocimeter (3C-LDV) allows us to characterise the flow. The 3C-LDV measures the speed of a seed particle as it goes through the measurement volume formed by the six laser beams. The tank is seeded with silver-coated glass micro-particles with a diameter of 10 µm. The 3C-LDV is placed at $(y, z) = (0, 0.5)H$ and measures the upstream velocity, in non-coincident mode, from $x/H = -1$ to $x/H = -8$, in EC (resp. FC) condition. At $x/H = -6$ the incoming flow is undisturbed by the Tidal Energy Converter (TEC) induction wathever the turbine

configuration. At this position, the mean streamwise velocity (noted U_0) is considered as the reference velocity. In flood and ebb tide configurations, the same reference velocity is kept: $U_0 = 0.85 \pm 0.02$ m/s. In addition, the Turbulent Intensity (TI) is controlled by setting up a grid and a honeycomb at the inlet of the test section (Figure 3). In all test cases presented here, TI is around 1.5%.

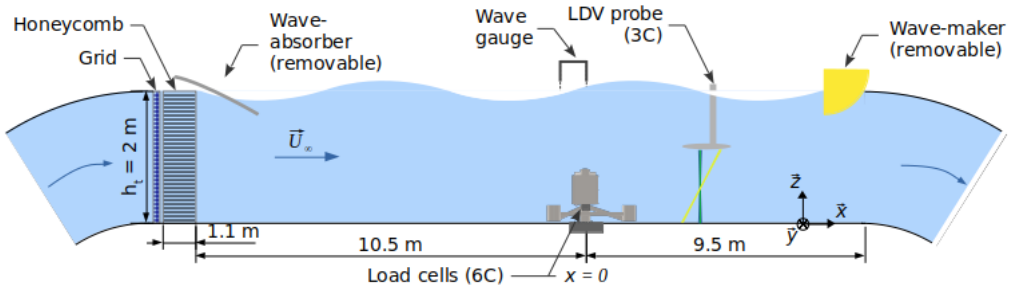

Figure 3. Ifremer wave and current flume tank experimental set-up view.

For the experimental campaign, a wave maker is used to generate surface waves in the tank [22]. To reduce the wave reflection, a wave absorber is positioned to the opposite of the wave maker in the working section. In this study, two wave cases are generated. Firstly, the wave maker is fixed at the inlet of the tank working section. In this configuration (noted FCW), the waves are following the current. Secondly, the wave maker is fixed at the outlet of the tank working section. In this configuration (noted ECW), the waves are propagating against the current. Two turbine orientations are tested in order to simulate the flood and ebb tide configurations (EC and FC). In FC, the counter-rotating rotor blades move against the flow along the central fairing, and the incoming flow encounters a single base pile, centered with the central part of the 2-VATT. In EC, the counter-rotating rotor blades move with the flow along the central fairing, and the incoming flow encounters two base piles, both aligned with the outer side of the areas swept by the rotors.

Above the 2-VATT at $(x, y) = (0,0)$, we placed a servo-type wave height meter (Kenek SHT3-30) and resistive wave probes to measure the free surface elevation (η) and the wavelength L. The properties of the wave cases used in this study are presented in Table 1, particularly, waves are characterized by their frequency f_h, wavelength L, and the time-averaged wave amplitude at the wave frequency η. In this study, we choose two cases of swell representative of the average to strong conditions encountered in the English Channel, with significant wave heights up to 5 m and pic period between 3 and 15 s [23].

Table 1. Characteristics of the wave cases generated in the flume tank.

	In the Flume Tank				At Sea	
	U_0 (m/s)	f_h (Hz)	η (m)	L (m)	H_s (m)	T_p (s)
ECW	0.8	0.4	0.10	4.9	3	11
FCW	0.8	0.75	0.07	4.3	4	6

For this study, Froude similarity ($Fr = \frac{U_0}{\sqrt{g(h_{wat} - H_{model})}}$) is considered to reproduce hydrodynamic conditions in the tank similar to the ones found at sea. The Froude number is around 0.24 at reduced scale and 0.17 at the Paimpol-Bréhat site, with a structure height of 17 m, a water depth of 40 m and a maximal current speed of about 2.5 m/s at full-scale. Based on the chord length, the Reynolds number, $Re_c = \frac{\lambda\, c\, U_0}{\nu}$ with $\nu = 1.05 \times 10^{-6}$ m^2/s the kinematic viscosity of the water, is about 5.2×10^6 in situ and 8×10^4 in the tank, which is approximately 60 times lower than at full scale. Due to the non-respect of Reynolds number

similarity, the performance of 2-VATT is underestimated [24], whereas wake development is not affected.

2.3. Data Acquisition and Processing

In order to compare our results with the ones obtained by [11] under a steady flow, we mapped the flow with the 3C-LDV system following the mesh on Figure 4 at x/H = {2, 3, 4, 5, 6, 7, 8, 9} at the turbine operating point (λ_{opt}), equal to 1.6 in flood tide configuration (FCW) and 1.5 in ebb tide configuration (ECW).

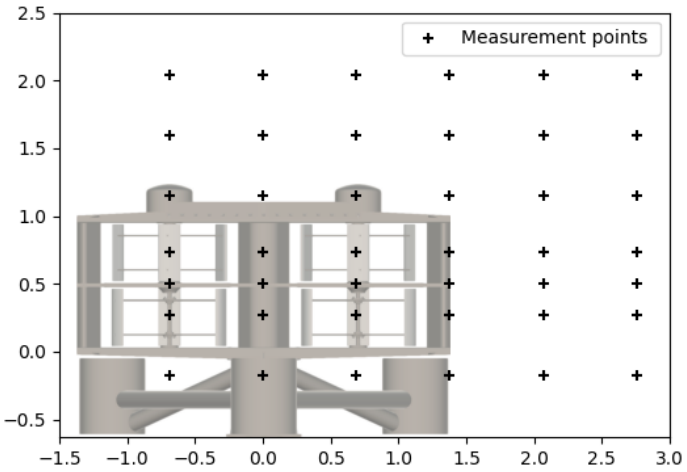

Figure 4. Velocity measurements mesh covered by the 3C-LDV probe.

At x/H = [0; 1], measurement planes are reduced because of the space required by the machine. The velocity maps presented below are based on linear interpolation between each measurement point. The interpolation step is 50 mm in the main direction (x) and 40 mm in the two other ones (y, z).

Synchronously, the rotational speed (ω), the torque (Q), and the load cell of each rotor column are acquired using National Instruments PXI and LabView systems at a sampling frequency of 128 Hz.

An acquisition time of three minutes is required to guarantee the signals mean and standard deviation convergence. The torque coefficient is calculated using Formula (1).

$$C_Q = \frac{Q(t)}{0.5\,\rho\,S_c\,R\,U_0^2},\ with\ S_c\ =\ 2\,D\,H_{blade} \tag{1}$$

The power coefficient (Cp) is extracted to measure the performance of the tidal turbine. The power coefficient is defined as Equation (2), as the ratio between the power extracted by each rotor column $P(=\sum \omega Q)$ and the power of the incoming flow P_∞.

$$Cp = \frac{P}{P_\infty} \quad = \quad \frac{P}{0.5\,\rho\,S\,U_0^3} \tag{2}$$

where ρ = 1000 kg m^{-3} the density of the water in the flume tank and S the projected surface of the four rotors (4 D H_{blade}). The Tip Speed Ratio (λ) can be also estimated (Equation (3)) and is calculated as follows:

$$\lambda = \frac{\omega\,R}{U_0} \tag{3}$$

A comparison is made at 0.8 m/s for the mean and standard deviation of C_p between EC and ECW. Therefore, the mean C_p curve is plotted depending on the mean tip speed ratio (Figure 5). Overall, the global performance of the 2-VATT shows that the mean value

is barely affected by the presence of surface waves, although a minor difference less than 8% is visible at λ_{opt}. However, the power fluctuations are significantly increased as λ increases with a difference in the standard deviation of around 32% at the optimal operating point (i.e., where the $\overline{C_p}$ is maximal). Ref. [25] showed that the increase in power fluctuations is related to an interaction between rotor rotation and surface waves.

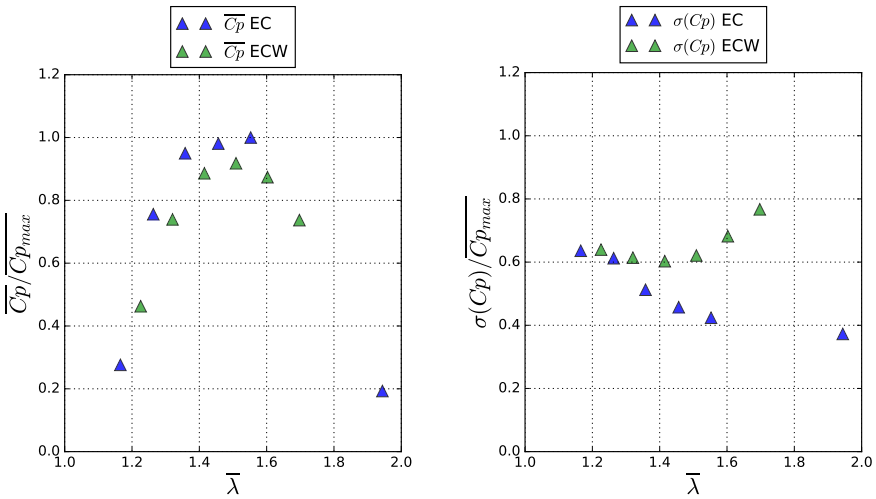

Figure 5. Power coefficient mean (**left**) and standard deviation (**right**) values in EC (blue curve) and ECW conditions (green curve).

It is well known that the frequency domain of hydrodynamic quantities is marked by a strong signal component around the wave frequency (f_h) [16,17,26], which means that these quantity fluctuations are mainly due to the wave-induced orbital velocity at f_h. Thus, the behaviour of the model is partially modified by the interaction with the waves.

To better understand the periodic variations in the torque of the 2-VATT induced by the waves, Figure 6 provides the Campbell diagram of the torque of the 2-VATT. It is noteworthy that at $\lambda \sim 1.5$ a transition occurs between the density contained at 6 times the rotation frequency (f_r) and the high density imposed by the surface waves at f_h. In fact, below λ_{opt}, the signal component at 6 f_r seems to predominate over the rest, whereas, for $\lambda > \lambda_{opt}$, the signal component at f_h largely dominates the spectral content of the torque. Therefore, when the tip speed ratio is high, the torque power distribution is fully driven by the wave-induced orbital velocity.

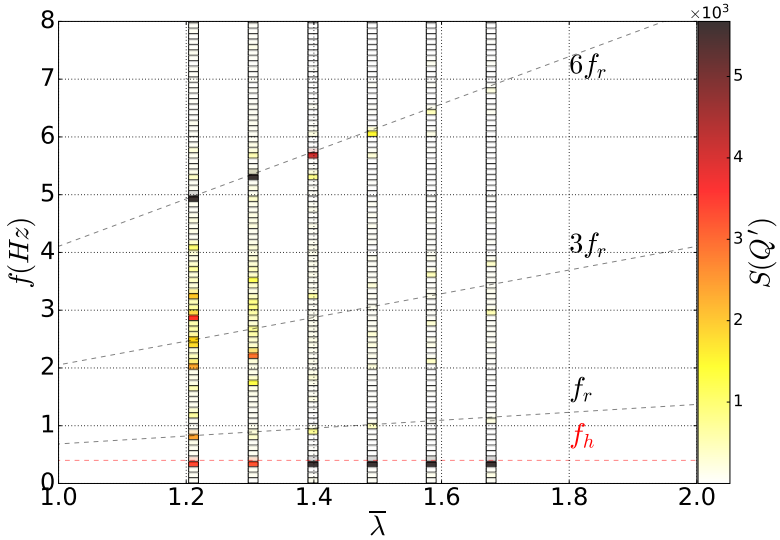

Figure 6. Campbell diagram of the torque of one rotor column of the 2-VATT with regard to the tip speed ratio in regular waves ECW.

Overall, the results show that 2-VATT's behaviour is wave-driven around the optimal operating point showin the necessity to study the wave effects on the wake development at λ_{opt}.

3. Wave Effects on the Turbine Wake Development

This section focuses on the wave–machine interaction and its impact on wake development. Thus, the following parts investigate the wave-induced modifications of its wake; first, by determining the evolution of the wake shape and then of its global dynamics. Detailed results are presented only for the ECW cases at λ_{opt} and the main results of the FCW case are discussed.

3.1. Wake Structures of the 2-VATT

Figure 7 presents an overview of the average axial velocity in the wake of the turbine in current only (EC) and regular waves (ECW) conditions. The wake exhibits a similar behaviour between EC and ECW close to the turbine ($x/H = 2$). In both cases a symmetrical distribution of the wake along the transverse axis is observed with the presence of the maximum velocity deficit behind each column of rotors. However, the development of the wake is different in both cases. Indeed, the low-momentum region featuring velocities below $0.5U_0$ diminishes more quickly in the ECW case.

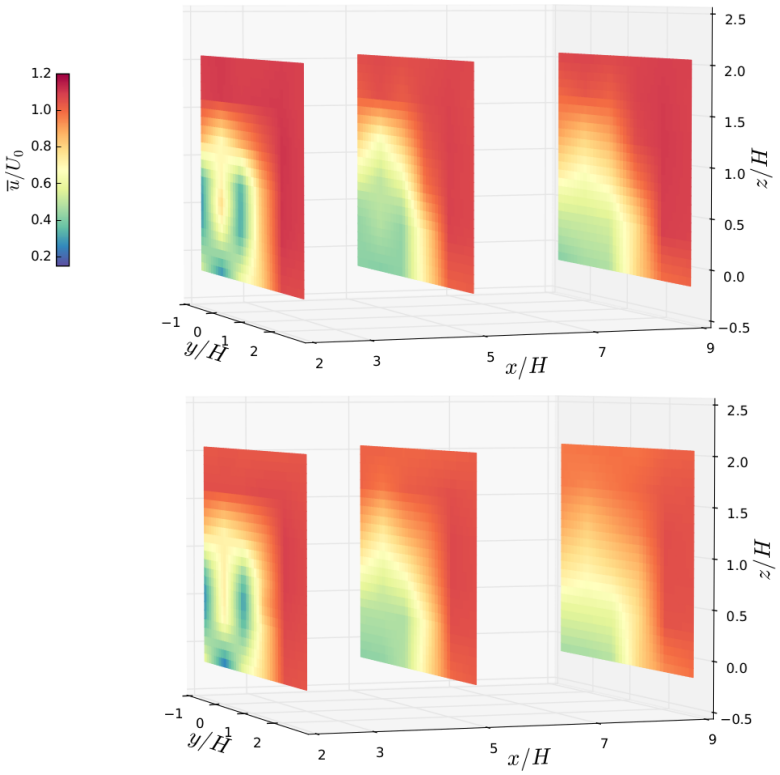

Figure 7. Average axial velocity ($\overline{u}/U_0$) at different locations in the wake of the turbine in the (x, y, z) plane in EC (**top**) and ECW (**down**). Axis origin is the center of the bottom horizontal plate of the turbine. Dimensions are scaled by the turbine height.

As a result, wake velocities in the presence of waves are generally higher than in the current-only cases with a velocity difference of around 12% behind the middle of the top rotor column (y/H = 0.69 and z/H = 0.5) at x/H = 5 and 8% at x/H = 9 (Figure 8). Moreover, the horizontal profiles (Figure 9) reveal that the velocity deficit present behind the rotor columns ($z/H = 0.5$) is more pronounced without wave propagation, with velocity differences in the order of 12% at $y/H = 0.69$ and $x/H = 5$ and 8% at $x/H = 9$. In other

words, the wave penetrates the 2-VATT's wake, resulting in an overall increase in velocity. Finally, the effect of the orbital component of the waves results in a significant rise of velocity fluctuations in the turbine's wake (Figures 8 and 9).

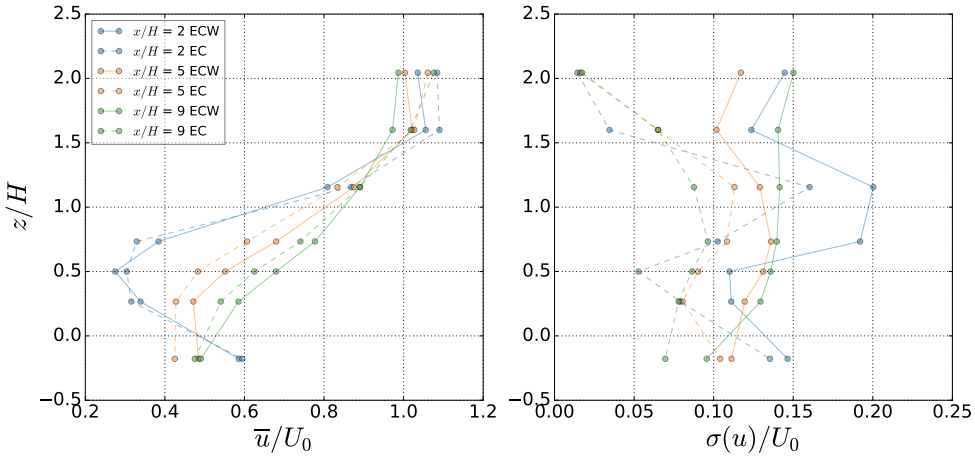

Figure 8. Streamwise velocity vertical profiles (mean (**left**) + standard deviation (**right**)) at $y/H = 0.69$ measured by LDV downstream of the turbine for different x-locations.

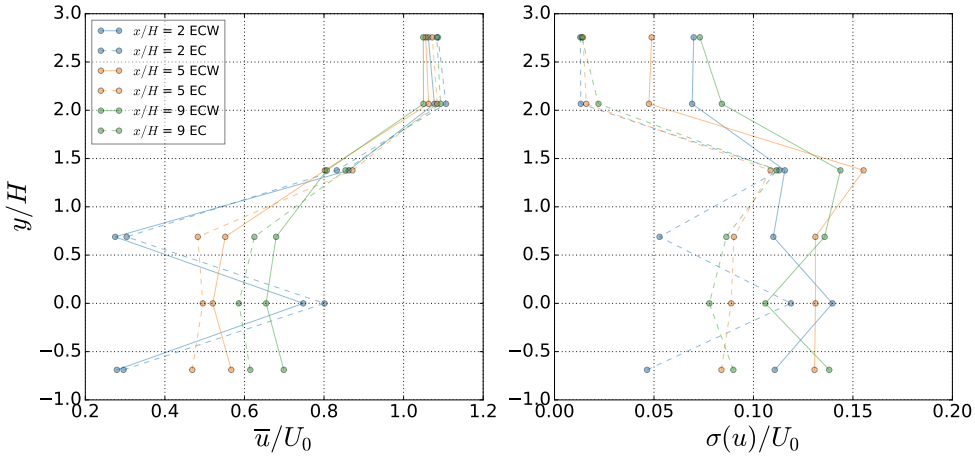

Figure 9. Streamwise velocity horizontal profiles (mean (**left**) + standard deviation (**right**)) at $z/H = 0.5$ measured by LDV downstream of the turbine for different x-locations.

Figures 10 and 11 display the normalized time-averaged streamwise velocity ($\overline{u}/U_0$) in (x, z) planes at y/H = 0.69 and in (x, y) planes at z/H = 0.5, respectively, in EC and ECW. Firstly, the (x, z) planes show good agreement between EC and ECW in the near wake (i.e., $x/H \leq 3$). In fact, the plans reveal a strong velocity deficit just behind the rotor column. Moreover, above the turbine, a high velocity zone can be observed due to the blockage effect in both cases. However, in the far wake, some differences can be noted, particularly with regard to the shape of the wake. Indeed, beyond x/H = 3, the contour levels reveal a slightly lower height of the wake in the presence of surface waves. Secondly, the (x, y) planes outline the wave effects on the overall wake behaviour of the 2-VATT. The maps unveil that the waves interfer with the turbine wake, which results in wakes merging, between the two rotor columns, closer to the free surface in EC than in ECW. Furthermore, the waves also cause a reduction in the propagation of the velocity deficit in the current direction.

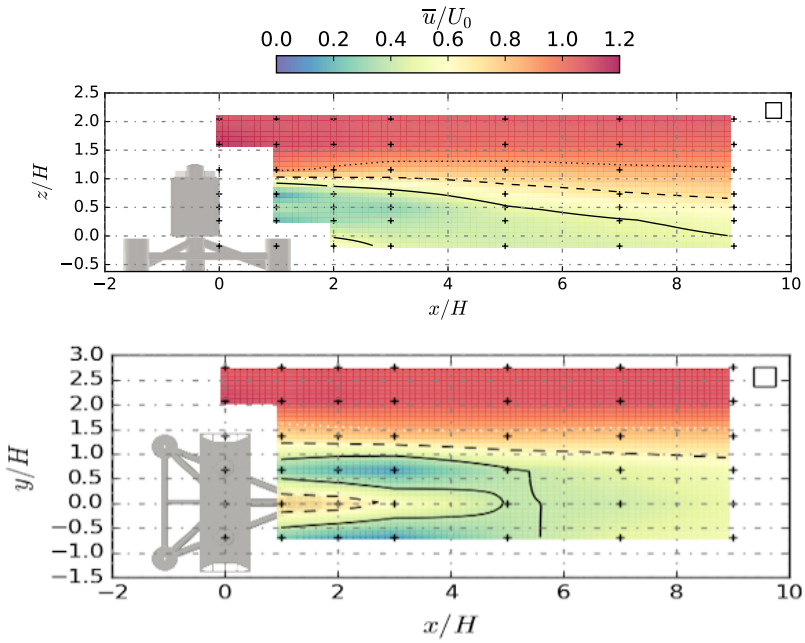

Figure 10. Two-dimensional wake maps of averaged velocity component ($\overline{u}/U_0$) in (x, z) planes at $y/H = 0.69$ (**top**) and in (x, y) planes at $z/H = 0.5$ (**bottom**) in EC. The solid, dashed, and dotted black lines are iso-contours of $\overline{u}/U_0 = 0.5$, 0.7, and 0.9, respectively.

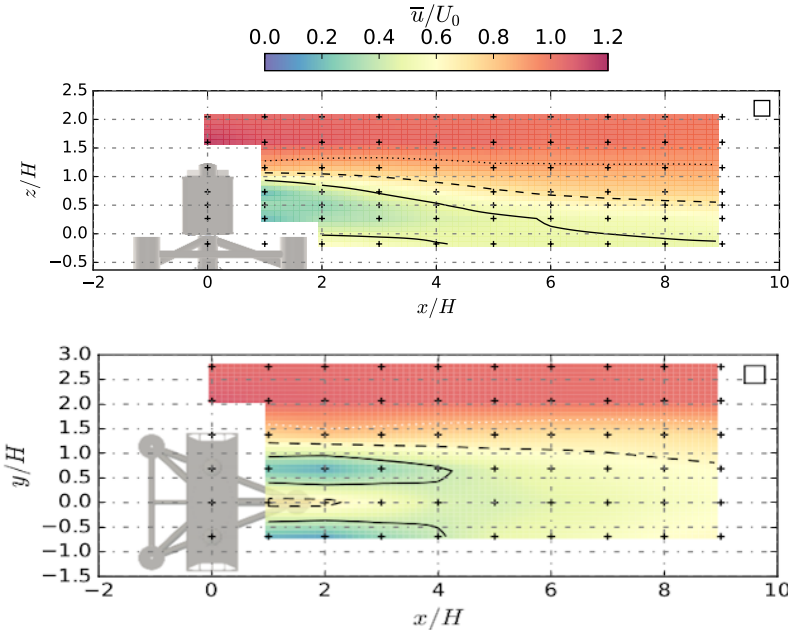

Figure 11. Two-dimensional wake maps of averaged velocity component ($\overline{u}/U_0$) in (x, z) planes at $y/H = 0.69$ (**top**) and in (x, y) planes at $z/H = 0.5$ (**bottom**) in ECW. The solid, dashed, and dotted black lines are iso-contours of $\overline{u}/U_0 = 0.5$, 0.7, and 0.9, respectively.

As it is commonly mentioned, the threshold of $\overline{u}/U_0 = 0.9$ is used to characterize the point at which the wake reaches its boundary [10]. Therefore, it is easy to study the average development of the wake height and width from this threshold. To do so, and in agreement with the studies of [11], Figure 12 displays the average wake height over the half turbine width $(0.00 < y/H < 1.38)$ by varying the downstream position in the EC and ECW. The average wake height is highly sensitive to wave action. In fact, the waves interfere with the wake, causing an increase in the turbine wake height. For all downstream positions, the wave effects are visibly reflected by an increase of around 11% of the average wake height at $x/H = 9$. The same observations were made in the case of regular waves

following the current, where the wake height is 11% greater in FCW than in FC. In the same way, Figure 12 illustrates the evolution of the average wake width over the turbine height $(0.00 < y/H < 1.00)$ of the wake boundaries of the 2-VATT for different x-positions. Similar to what we saw for the height, the width of the wake is modified by the presence of the waves. Indeed, we see an increase in wake width from $x/H = 2$ to $x/H = 9$. However, the impact of the wave is more pronounced in the far wake of the 2-VATT with a wake width being 4% wider at $x/H = 2$ and of around 12% wider at $x/H = 9$ in comparison to EC. The results obtained in the flood tide configuration show that the FCW cases have an average wake width that is 5% wider at $x/H = 2$ and around 11% wider at $x/H = 9$ than the FC cases.

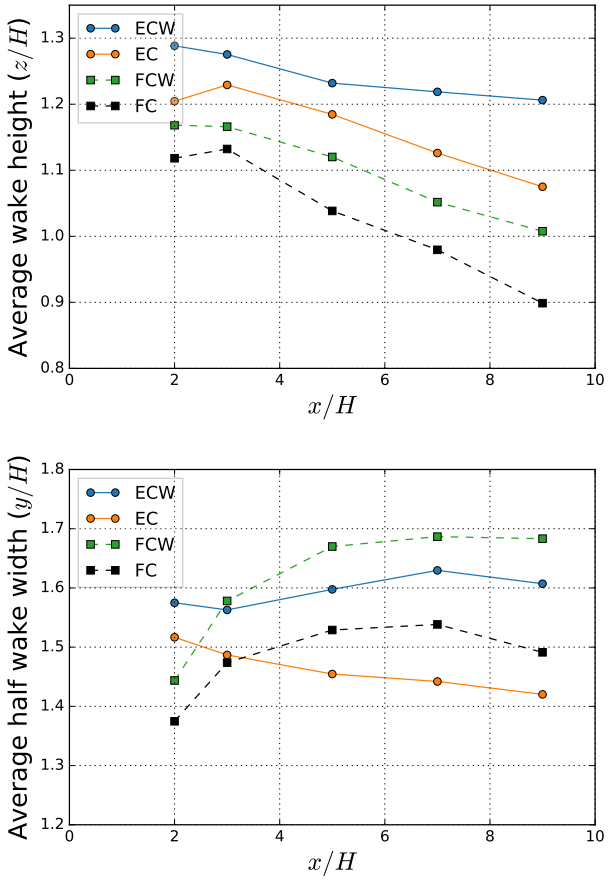

Figure 12. Comparison of the evolution of the wake height (**top**) and width (**bottom**) as a function of the x-position for all the test cases.

To complete the time-averaged wake dynamics, another tool is used. It details the phenomena underlying the modification of the wake by the waves. To this aim, the average velocity fields are calculated at different phase instants to understand how the wave-induced orbital velocity influences the wake development. A comparison of the time average and the average over a wave period confirmed the validity of the results.

Figure 13 presents the phase average of the streamwise velocity, for five phase instants, from $-\pi$ to π. At $\phi = -\pi$, the wave trough passes over the head of the tidal turbine and $\phi = 0$ corresponds to the wave crest. As it can be observed, the wave propagation is underlined by an alternation of low and high streamwise velocity components close to the free surface induced by the transition between the crest and the trough of the wave. In fact, in these zones the orbital velocity is sometimes in the direction of the current (trough) and other times against the current (crest).

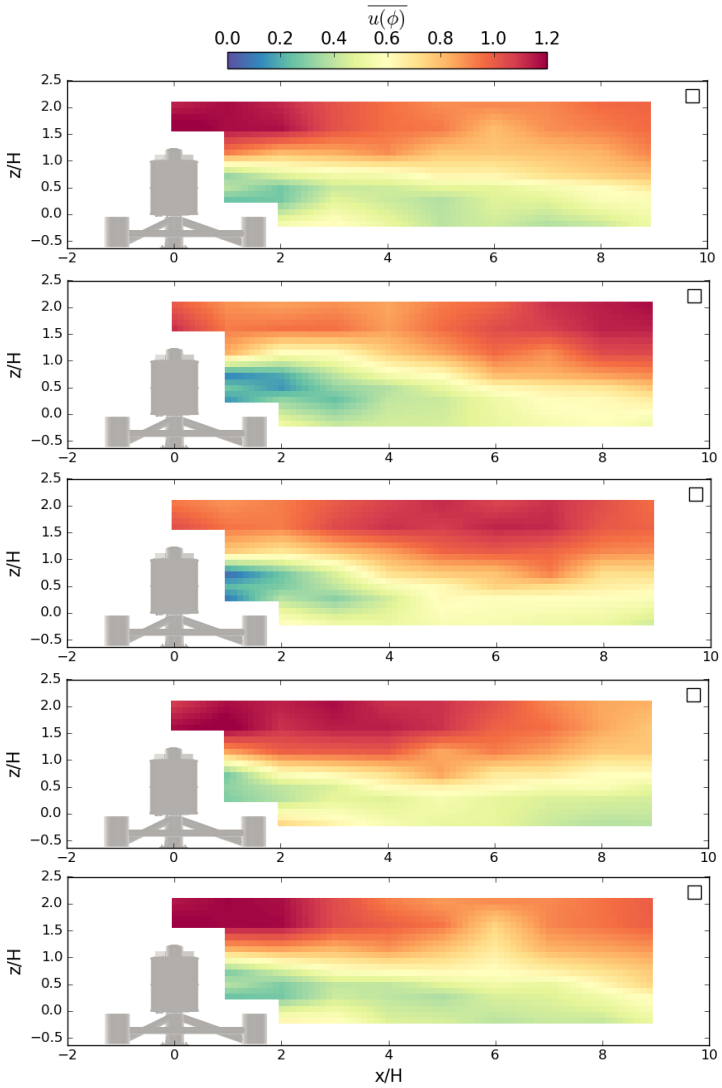

Figure 13. Phase average of current velocity in the ECW at wave frequency f_h at $y/H = 0.69$ from $-\pi$ to π by $\pi/2$ increments.

In the figure, as the wave front rises (from trough to crest), the near-wake tends to move towards the surface due to the high intensity of the orbital velocity in the z-direction. On the opposite, when the wave is moving downwards (from crest to trough), the wake of the 2-VATT is pushed against the bottom of the flume tank. This phenomenon is still clearly visible in Figure 14, exhibiting the contour plot of the phase average streamwise velocity, for five phases. It can be seen that the wake shape evolution is a function of the wave phase. Unlike the stationary case, the presence of waves disturbs the 2-VATT's wake development at the wave frequency. The turbine wake is first raised towards the free surface and then crushed against the floor of the tank.

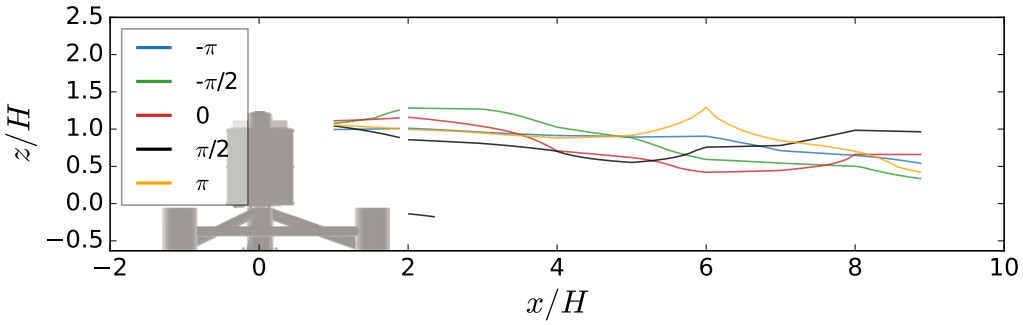

Figure 14. Contours plot of the phase average streamwise velocity, for five phase, with regard to the phase ϕ. the contour is made for $\overline{u(\phi)} \leq 0.7$.

To sum up, the maximum velocity deficit is defined as all velocity $\overline{u(\phi)} \leq 0.5$. Thus, Figure 15 displays the evolution of the maximum velocity deficit as a function of the wave phase. We noted that the evolution of the maximum velocity deficit is $\pi/2$ out of phase with η. Indeed, the lowest velocities are encountered when the transition between trough and crest occurs whereas the highest velocity is observed after the passage of the wave crest. The difference between the local min and max velocity deficit is about 18%. Thus, phase averaging reveals a significant change in wake shape, which can lead to significant velocity fluctuations and alter wake dynamics.

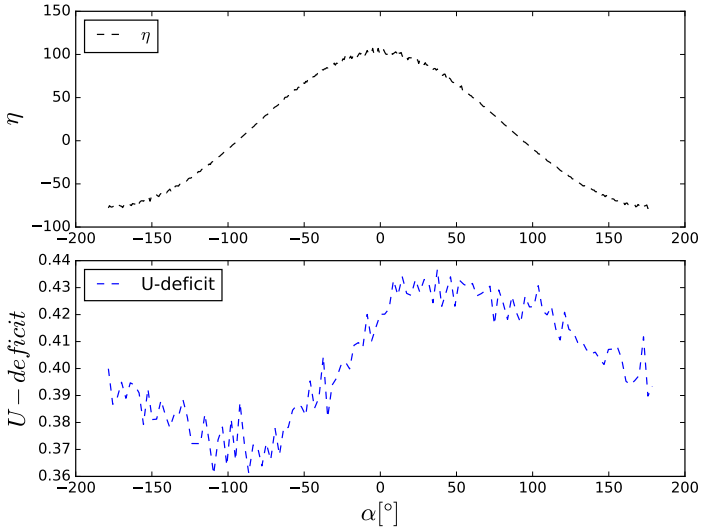

Figure 15. Evolution of maximum velocity deficit $\overline{u(\phi)} \leq 0.5$ versus surface elevation η. Mean values are only calculated for distances $x = 2$ to 9 H.

3.2. Wake Dynamics and Recovery

Figure 16 displays the mean u-velocities contours with superimpositions of arrow fields of the mean transverse velocities $(\overline{v}, \overline{w})/U_0$. Thus, we can compare the wake dynamics between the EC and ECW. The arrow fields illustrate that in the ECW the ambient flow is entrained more strongly in the turbine wake by the presence of two swirls with higher v and w components than in the EC. These wake swirls are created by the velocity gradient formed by the different layers in the wake and are intended to compensate for the velocity deficit in the wake of the 2-VATT. Thus, the formation of these swirls is associated with a reduction in the volume of the wake. This impact is more pronounced in the ECW due to the presence of more structured and persistent swirls in the wake.

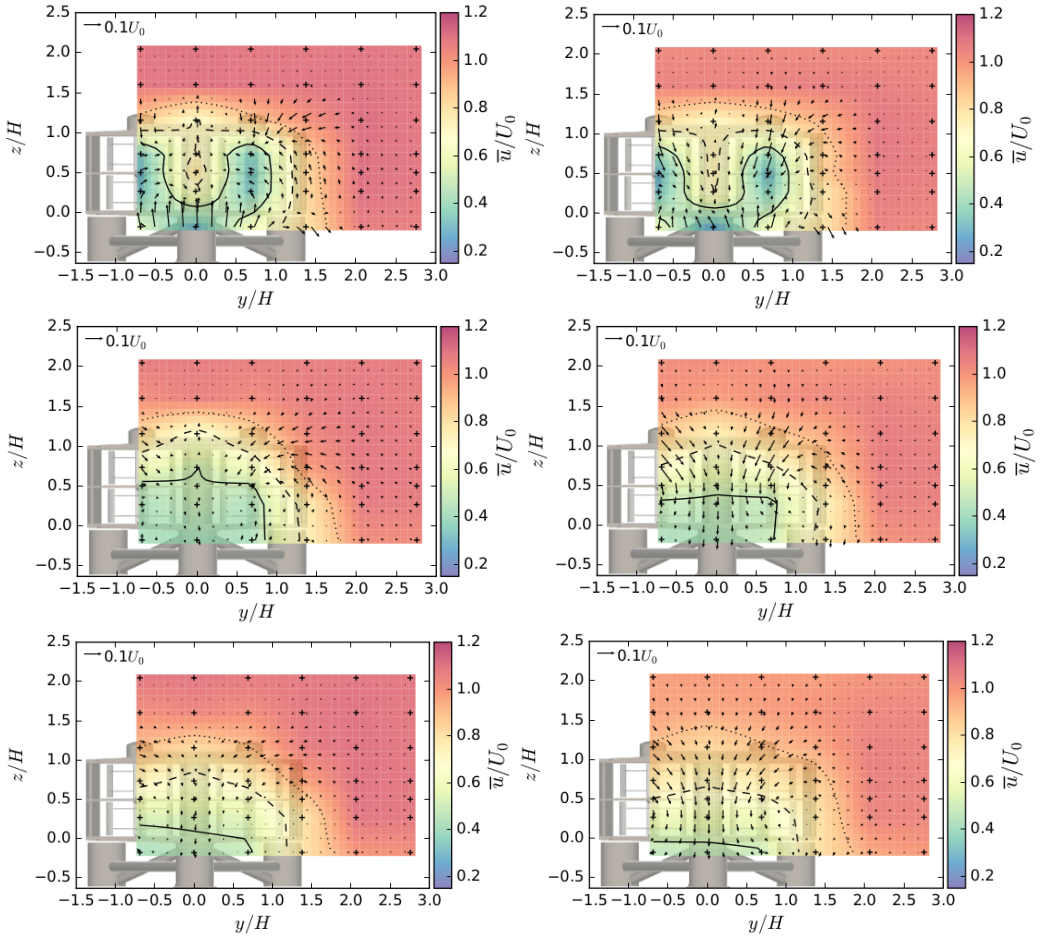

Figure 16. Mean streamwise velocity contours in transverse planes, with arrow field of the mean transverse velocities $(\overline{v}, \overline{w})/U_0$ superimposition in EC (**left**) and ECW (**right**) for three different downstream locations (from **top** to **bottom**: $x/H = 2$ $x/H = 5$ and $x/H = 9$). The solid, dashed, and dotted black lines are iso-contours of $\overline{u}/U_0 = 0.5, 0.7$, and 0.9, respectively.

This can also be seen on the horizontal profiles of the mean vertical velocities (Figure 17), where the transverse velocity w is more important in ECW than in EC. Therefore, the waves tend to flatten the wake against the bottom of the flume tank, explaining that the maximum velocity deficit is less pronounced in ECW.

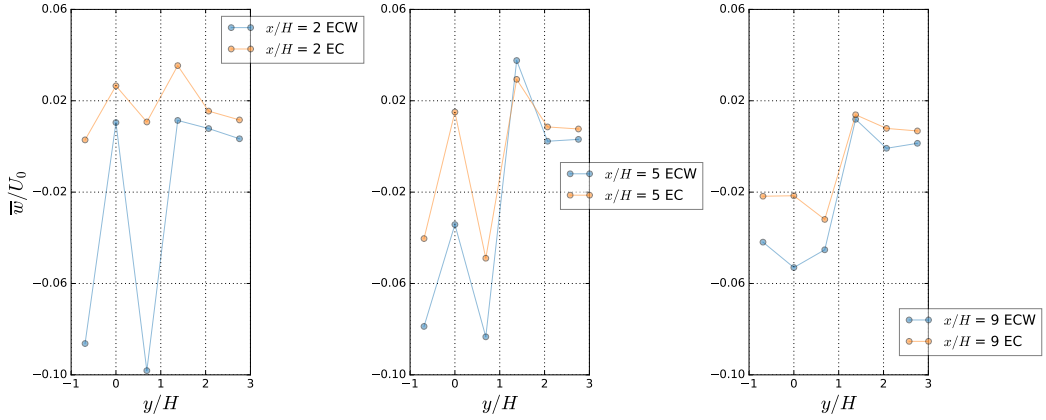

Figure 17. Horizontal profiles at mid-height of the upper rotor of the mean vertical velocity at different distances downstream of the turbine.

To sum up, the normalised 3D Turbulence Kinetic Energy (TKE), expressed as $TKE = \frac{1}{2U_0^2}(\overline{u'^2} + \overline{v'^2} + \overline{w'^2})$, in (y, z) planes is shown in Figure 18. In both cases, TKE is more

intense in the near wake ($x/H \leq 3$) close to the turbine's upper quadrant and on the tips of the rotors. This aspect can be explained by the bypass of the flow above the 2-VATT and to the tip vortices shedding [27]. The magnitude of TKE decreases with downstream position, almost disappearing at $x/H = 9$ in EC. However, in ECW the TKE remains significant with a highly energetic area of energy between the turbine and the free surface, which is explained by the interaction that occurs between the purely turbulence-induced velocity and the wave-induced orbital velocity, resulting in a larger momentum in ECW. This highlights the injection of energy by the waves in the wake of the 2-VATT, which leads to better flow mixing between the external region and the wake in ECW than in EC.

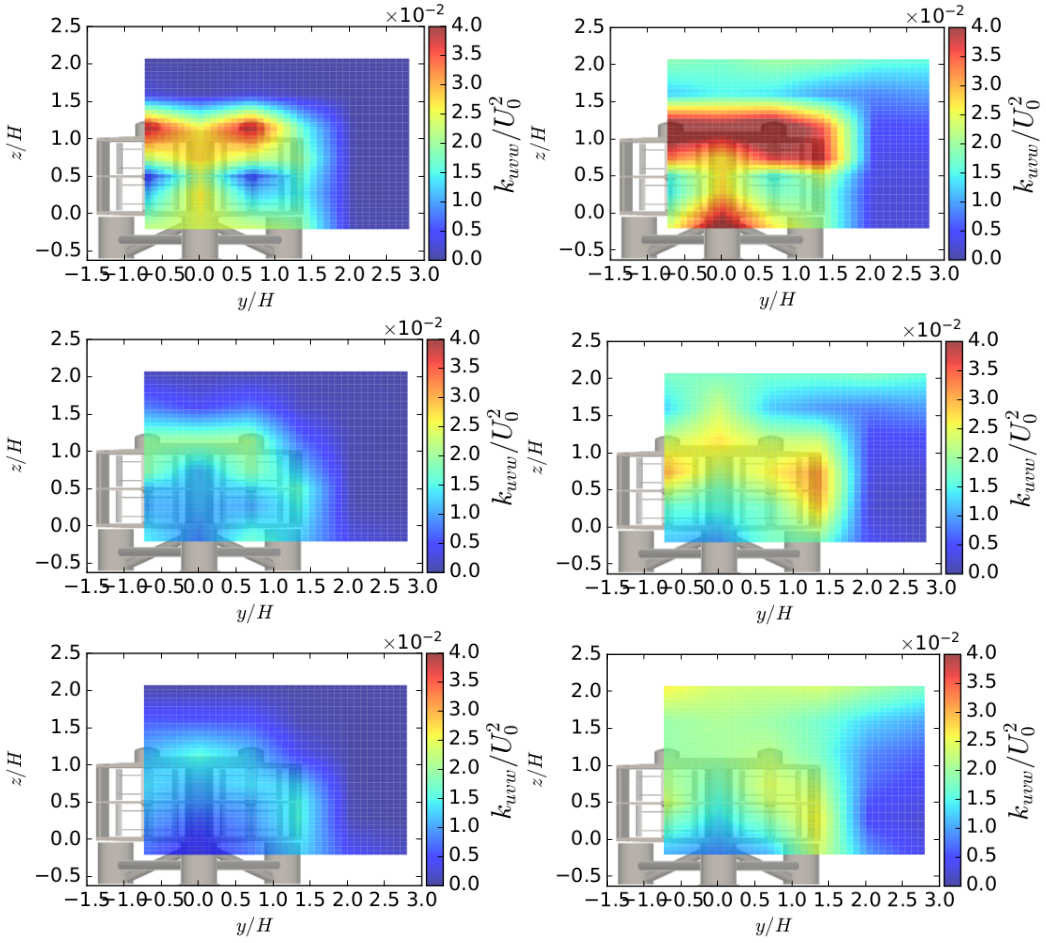

Figure 18. Maps of the normalized Fluctuating Kinetic Energy (TKE) in (y, z) plane, respectively, from top to bottom at x/H = 2, 5 and 9 in EC (**left**) and under wave conditions (**right**).

The global behaviour of the wake downstream of the turbine can be summarized by calculating the surface average of the time-averaged variable. Figures 19 and 20 display the surface average of the mean streamwise velocity and the turbulent kinetic energy over the wake region delimited by $0.9U_0$ in the EC and ECW. It is notable that the ECW has a higher longitudinal velocity intensity compared to the EC case. This can be attributed to the orbital velocity induced by the waves, which tends to increase the wake dynamics. In fact, the results show a smaller difference (around 1.5%) between the current-only and wave cases from x/H = 2 to 3. Beyond x/H = 3, the waves induce 4.5% faster wake recovery compared to the current-only case. In other words, wake strength appears significantly weaker in the ECW configuration than in the EC configuration in the far wake.

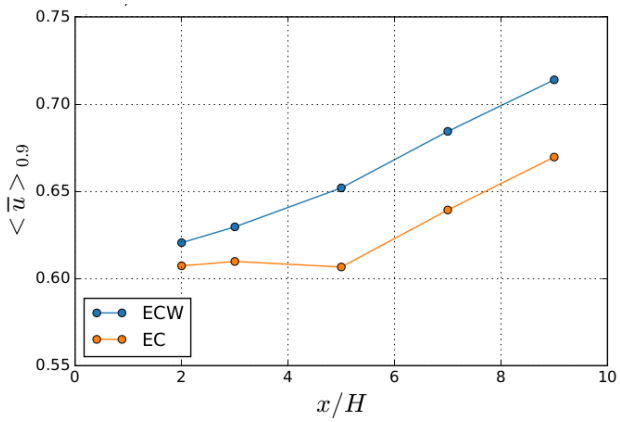

Figure 19. Spatial average of the mean streamwise velocity over the wake region delimited by $0.9U_0$ in EC and ECW.

Figure 20 exhibits that the surface averaged of the TKE is more intense in the ECW than in the EC. Indeed, as mentioned above, the wake of the 2-VATT is continuously modified by the presence of waves, resulting in a series of periodic velocity variations close to the free surface (Figure 13). This effect induces high velocity fluctuations in this zone, as shown in Figure 18, and leads to an overall increase in kinetic energy in the turbine's wake. In addition to the turbulent kinetic energy produced by the passage of the waves, the wave maker is responsible for releasing coherent structure, which has the effect of further increasing the TKE.

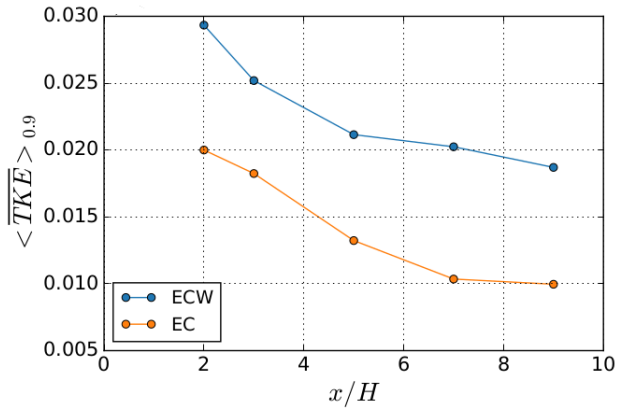

Figure 20. Spatial average of the turbulent kinetic energy over the wake region delimited by $0.9U_0$ in the EC and ECW.

4. Conclusions

This paper aims to provide clarification on the effect of the surface waves on a ducted twin vertical axis tidal turbine (2-VATT) performance and wake development. To this aim, we tested a 1/20 scale model of the 1 MW-rated demonstrator tested at Paimpol-Bréhat test site facing surface waves propagating against the current.

The results show that the average power coefficient of the ducted turbine is unaffected by the surface waves. However, the torque spectral content reveals a large domination of the wave frequency for the high TSR level and so the power coefficient standard deviation is 32% higher at the optimal operating point with regular waves compared to the current-only cases.

As regards to the flow downstream of the turbine, the wake is modified by the waves which, in the far wake, present an average height and width approximately 11% higher in the presence of surface waves. The presence of two swirling structures around the x-axis are observed in both cases. These swirls are stronger and more resistant under the wave action, introducing a stronger momentum between the ambient flow and the wake of the ducted

twin vertical axis tidal turbine and leading to a higher rate of wake recovery in the presence of waves. Thus, the overall wake recovery of the 2-VATT is 4.5 % faster in ECW than in EC. Although the waves favour better mixing of the turbine wake, fluctuations in velocity subsist over a long distance downstream of the tidal turbine. The phase-averaged velocity has also shown that the passage of a wave drives the development of the wake, with varying degrees of deformation. It has been shown that over the wave period, the wake is both aspirated towards the free surface and pressed against the bottom of the flume tank. These periodic variations also lead to a temporal evolution in the dissipation of the maximum velocity deficit.

In this work, only two wave cases have been considered. Additional tests with different wave frequency, amplitude, and direction could help to generalized this study. It will be then possible to quantify the wave effects on the behaviour (performance and wake development) of tidal turbines whatever the kind of considered technologies.

Author Contributions: Conceptualization, G.G. and G.M.; methodology, R.L., Y.S., G.G. and G.M.; software, R.L. and Y.S.; validation, G.G. and G.M.; formal analysis, R.L.; investigation, R.L. and G.G.; resources, G.G. and G.M.; data curation, R.L. and Y.S.; writing—original draft preparation, R.L.; writing—review and editing, R.L. and G.G.; visualization, R.L.; supervision, G.G. and G.M.; project administration, G.G. and G.M.; funding acquisition, G.G. and G.M. All authors have read and agreed to the published version of the manuscript.

Funding: This work received the financial support of the French Agence Nationale de la recherche through the Verti-Lab project (ANR-23-LCV1-0009-01) and of the French Research and Technology National Association (ANRT) under the convention Cifre n°2023/0217. This research was also partly funded by the Région Hauts-de-France in the framework of the project CPER 2021–2027 IDEAL.

Data Availability Statement: The research data as well as the complete drawings of the model can be available upon request to the authors.

Acknowledgments: The authors acknowledge JV. Facq, B. Gaurier and B. Gomez for their help during the experiments.

Conflicts of Interest: The authors declare no conflicts of interest.

Abbreviations

The following abbreviations are used in this manuscript:

U_0	Reference velocity measured far upstream of the turbine
H_s	Significant wave height
H	Top to bottom horizontal plates distance of Gen1's fairing
FC	Flood Tide Configuration
EC	Ebb Tide Configuration
h_{wat}	Depth of the flume tank
w_{wat}	Width of the flume tank
η	Free surface elevation
T_p	Wave peak period
A_η	Significant wave amplitude
λ	Tip speed ratio
λ_{opt}	Refers to tests at the operating point providing the maximal C_P
f_h	Wave frequency
L	Wavelength
TKE	Turbulent kinetic energy
S_c	Reference surface taken as a rotor column's one

References

1. Neill, S.; Haas, K.; Thiébot, J.; Yang, Z. A review of tidal energy—Resource, feedbacks, and environmental interactions. *J. Renew. Sustain. Energy* **2021**, *13*, 18. [CrossRef]
2. O'Rourke, F.; Boyle, F.; Reynolds, A. Ireland's tidal energy resource; An assessment of a site in the Bulls Mouth and the Shannon Estuary using measured data. *Energy Convers. Manag.* **2014**, *87*, 726–734. [CrossRef]
3. Thomson, J.; Polagye, B.; Durgesh, V.; Richmond, M. Measurements of Turbulence at Two Tidal Energy Sites in Puget Sound. *IEEE J. Ocean. Eng.* **2012**, *37*, 363–374. [CrossRef]
4. Lewis, M.; Neill, S.P.; Robins, P.E.; Hashemi, M.R. Resource assessment for future generations of tidal-stream energy arrays. *Energy* **2015**, *83*, 403–415. [CrossRef]
5. Brevik, I.; Bjørn, A. Flume experiment on waves and currents. I. Rippled bed. *Coast. Eng.* **1979**, *3*, 149–177. [CrossRef]
6. Kumar, A.; Hayatdavood, M. On wave–current interaction in deep and finite water depths. *J. Ocean. Eng. Mar. Energy* **2023**, *9*, 455–475. [CrossRef]
7. Bahaj, A.; Myers, L.; Thomson, M.; Jorge, N. Characterising the wake of horizontal axis marine current turbines. In Proceedings of the 7th European Wave and Tidal Energy Conference, EWTEC, Porto, Portugal, 11–13 September 2007.
8. Pinon, G.; Mycek, P.; Germain, G.; Rivoalen, E. Numerical simulation of the wake of marine current turbines with a particle method. *Renew. Energy* **2012**, *46*, 111–126. [CrossRef]
9. Mycek, P.; Gaurier, B.; Germain, G.; Pinon, G.; Rivoalen, E. Experimental study of the turbulence intensity effects on marine current turbines behaviour. Part I: One single turbine. *Renew. Energy* **2014**, *66*, 729–746. [CrossRef]
10. Ebdon, T.; Allmark, M.; O'Doherty, D.; Mason-Jones, A.; O'Doherty, T.; Germain, G.; Gaurier, G. The impact of turbulence and turbine operating condition on the wakes of tidal turbines. *Renew. Energy* **2021**, *165*, 96–116. [CrossRef]
11. Moreau, M.; Germain, G.; Facq, J.V.; Maurice, M.; Derveaux, C. Experimental study of two opposed flow directions effect on a ducted twin vertical axis tidal turbine. In Proceedings of the European Wave and Tidal Energy Conference, EWTEC, Bilbao, Spain, 3–7 September 2023.
12. Müller, S.; Muhawenimana, V.; Wilson, C.; Ouro, P. Experimental investigation of the wake characteristics behind twin vertical axis turbines. *Energy Convers. Manag.* **2021**, *247*, 114768. [CrossRef]
13. Ouro, P.; Dené, P.; Garcia Novo, P.; Stallard, T.; Kyozuda, Y.; Stansby, P. Power density capacity of tidal stream turbine arrays with horizontal and vertical axis turbines. *J. Ocean. Eng. Mar. Energy* **2022**, *9*, 203–218. [CrossRef]
14. Luznik, L.; Flack, K.; Lust, E.; Taylor, K. The effect of surface waves on the performance characteristics of a model tidal turbine. *Renew. Energy* **2013**, *58*, 108–114. [CrossRef]
15. Lust, L.; Luznik, L.; Flack, K.; Walker, J. The influence of surface gravity waves on marine current turbine performance. *Int. J. Mar. Energy* **2013**, *3*, 27–40. [CrossRef]
16. Gaurier, B.; Davies, P.; Deuff, A.; Germain, G. Flume tank characterization of marine current turbine blade behaviour under current and wave loading. *Renew. Energy* **2013**, *59*, 1–12. [CrossRef]
17. de Jesus Henriques, T.; Tedds, S.; Botsari, A.; Najafian, G.; Hedges, T.; Sutcliffe, C.; Owen, I.; Poole, R. The effects of wave–current interaction on the performance of a model horizontal axis tidal turbine. *Int. J. Mar. Energy* **2014**, *8*, 17–35. [CrossRef]
18. Lin, X.; Zhang, J.; Guan, D.; Zhang, C.; Gan, M. Wake Characteristics of a Tidal Stream Turbine under Combined Wave and Current. *J. Coast. Res.* **2020**, *95*, 1558–1562. [CrossRef]
19. Zhang, Y.; Zang, W.; Zheng, J.; Cappietti, L.; Zhang, J.; Zheng, Y.; Fernández-Rodríguez, E. The influence of waves propagating with the current on the wake of a tidal stream turbine. *Appl. Energy* **2021**, *290*, 116729. [CrossRef]
20. Stallard, T.; Mullings, H.; Draycott, S.; Ouro, P. Large-eddy simulations of interaction between surface waves and a tidal turbine wake in a turbulent channel. In Proceedings of the European Wave and Tidal Energy Conference, EWTEC, Bilbao, Spain, 3–7 September 2023; Volume 15.
21. Moreau, M.; Germain, G.; Maurice, G.; Richard, A. Sea states influence on the behaviour of a bottom mounted full-scale twin vertical axis tidal turbine. *Ocean. Eng.* **2022**, *265*, 112582. [CrossRef]
22. Magnier, M.; Gaurier, B.; Germain, G.; Druault, P. Analysis of the wake of a wide bottom-mounted obstacle in presence of surface wave following tidal current. In *Trends in Renewable Energies Offshore*; CRC Press: Boca Raton, FL, USA, 2022; pp. 151–159.
23. Hardwick, J.; Mackay, E.; Ashton, I.; Smith, H.; Thies, P. Quantifying the Effects of Wave—Current Interactions on Tidal Energy Resource at Sites in the English Channel Using Coupled Numerical Simulations. *Energies* **2021**, *14*, 3625. [CrossRef]
24. Ross, H.; Polagye, B. Effects of dimensionless parameters on the performance of a cross-flow current turbine. *J. Fluids Struct.* **2022**, *114*, 103726. [CrossRef]
25. Moreau, M.; Germain, G.; Maurice, G. Experimental Investigation of Surface Waves Effect on a Ducted Twin Vertical Axis Tidal Turbine. *J. Mar. Sci. Eng.* **2023**, *11*, 1895. [CrossRef]

26. Draycott, S.; Steynor, J.; Nambiar, A.; Sellar, B.; Venugopal, V. Rotational sampling of waves by tidal turbine blades. *Renew. Energy* **2020**, *162*, 2197–2209. [CrossRef]
27. Bachant, P.; Wosnik, M. Characterising the near-wake of a cross-flow turbine. *J. Turbul.* **2015**, *16*, 392–410. [CrossRef]